Caving 2026 – A van As, D Cumming-Potvin & J Wesseloo (eds)

doi:10.36487/ACG_repo/2645_86

Findings from large-scale distributed acoustic sensing monitoring of the Panel 0 block cave at Oyu Tolgoi

Wille Törnman [a,b,*], Jesper Martinsson [a], Erdenetogtokh Bayar [c], Munkh-Erdene Ulziijargal [c], Batbandi Uranchimeg [c], Charles Lilley [d], Andy Davies [e], Mohammad Amir [f], Emil Svanberg [a]

[a] *RockSigma, Sweden*

[b] *Luleå University of Technology, Sweden*

[c] *Oyu Tolgoi LLC, Mongolia*

[d] *Rio Tinto, Australia*

[e] *Rio Tinto, USA*

[f] *Silixa, UK*

Abstract

This paper presents key findings from a large-scale deployment of distributed acoustic sensing (DAS) for seismic monitoring at an active block cave mine. The fibre-optic cables were installed in boreholes positioned to the side of the cave footprint to enable continuous monitoring of both strain and seismic activity throughout cave propagation. The system was designed to remain operational as the cave expanded, providing a rare opportunity to observe the evolution of seismic response in real time. The installation initially comprised 398 DAS channels, generating a large data volume that demonstrated the scalability and real-time performance of the processing software. Despite a suboptimal geometry for event location, with two nearly parallel boreholes, the end-to-end system successfully captured microseismic signals and located seismic events reflecting the stages of cave development. Using fibre optics also allows microseismic data to be integrated with strain and distributed strain sensing (DSS) measurements for enhanced interpretation. Overall, the study confirms that DAS is a viable and scalable tool for continuous, high-resolution seismic monitoring in block cave environments, and it highlights that sensor geometry should be carefully considered in the design phase to optimise event localisation and interpretive value.

Keywords: *distributed acoustic sensing, block caving, microseismic monitoring, fibre-optic sensing, cave propagation, sensor geometry*

1 Introduction

Cave propagation in block cave mines triggers seismicity which must be monitored to manage safety risks, estimate the cave geometry and understand the mechanics of cave propagation. Seismic monitoring is therefore critical for block cave mines (Bayar et al. 2024). Traditionally this monitoring has been done with point-sensor arrays, but distributed acoustic sensing (DAS) has now emerged as a promising alternative.

Distributed fibre optic sensing, including DAS, uses standard optical fibre as a continuous sensor, enabling measurements along its entire length from a single interrogator unit.

By using fibre-optic cables, DAS allows for continuous monitoring along the entire length of the fibre (Lindsey et al. 2017). For the mining industry, this technology offers several advantages compared to conventional geophone or accelerometer-based networks. The fibre installation is relatively inexpensive, requires no power or communication infrastructure near the sensing points, and removes the time synchronisation issues often found in wired networks (Lindsey et al. 2017). In addition, DAS systems provide a broad frequency

* Corresponding author. Email address: wille.tornman@rocksigma.com

response, reducing the need for precise sensor frequency selection and mitigating uncertainties related to rock mass attenuation characteristics. Furthermore, silica-based fibres have a long life span with minimal degradation if they are properly installed and protected. Spatial coverage can often be obtained by reusing pre-existing boreholes. Maintenance is also simplified since the system uses a single interrogator unit that can be placed in a safe location, away from active mining.

However, adopting DAS in a block caving context also brings new challenges. The volume of waveform data is very large, which creates hurdles for data transfer and requires significant computational power for real-time processing. DAS also has particular noise characteristics and directional sensitivity; for example, P-waves arriving perpendicular to the fibre are often poorly recorded, making traditional processing workflows more challenging. Additionally, the geometry of fibre installations can lead to 'mirroring effects' and location ambiguities (Martinsson 2013; Törnman et al. 2024), particularly for smaller seismic events.

This paper presents the key findings from a large-scale deployment of DAS at the Oyu Tolgoi underground mine in Mongolia, specifically between Panel 0 (P0) and Panel 2 North (P2N) of Hugo North Lift 1. At the time of installation, this volume of rock was expected to form a pillar as the P2N cave propagated. To enable continued monitoring as caving progressed, the boreholes were equipped with optical turnarounds at depths of 33, 66 and 100% of the total depth. This redundancy ensures that monitoring capability is maintained in the upper sections even as the lower sections are compromised. The objective is to evaluate how the system performs as the cave propagates. We discuss the specific challenges encountered, such as geometry constraints and data processing needs, and demonstrate that DAS is a viable and scalable tool for high-resolution seismic monitoring in complex mining environments, although cable damage ultimately limited the ability to monitor the anticipated pillar as originally planned.

2 Site and installation overview

This section summarises the operational context and monitoring configuration at the P0 block cave. The system was designed to withstand active cave propagation while enabling dual distributed strain sensing (DSS) and seismic DAS measurements in a challenging underground environment.

2.1 Oyu Tolgoi Panel 0 block cave overview

The monitoring infrastructure is located to the south of P0, as shown in Figure 1. This location was selected primarily to observe strain accumulation and rock mass response along the fibres using DSS. Although the resulting borehole geometry is not optimal for seismic hypocentre estimation with DAS, it provides valuable insight into how seismicity evolves as the cave expands and interacts with the surrounding rock mass.

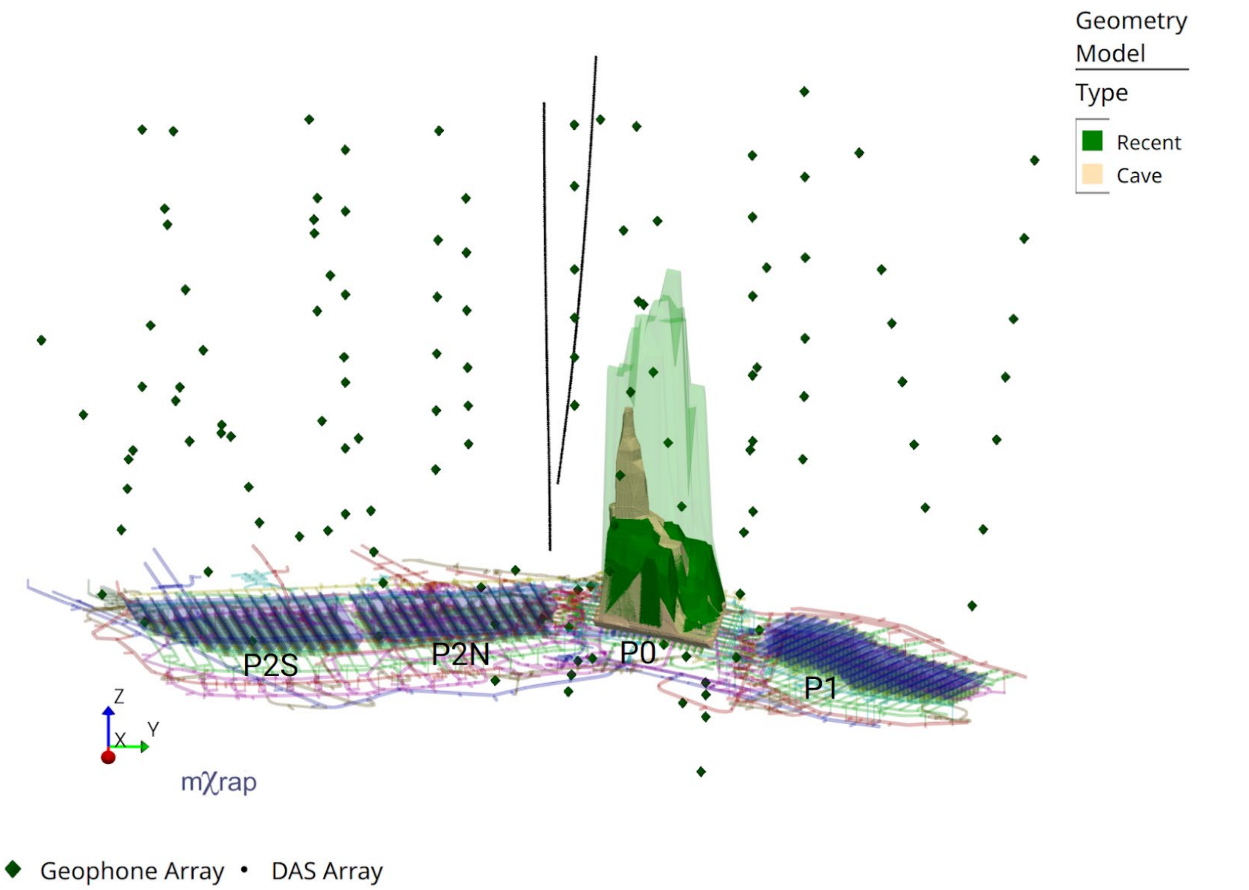

Figure 1 3D view showing the location of the mine panels and monitoring arrays. Panel 0 (P0) is in production, Panel 2 North (P2N) is under development, and P2S and P1 are planned future development areas within the western infrastructure precinct. The development geometry at the time of this study is shown in beige and dark green, with a more recent geometry from June 2025 shown in transparent green for reference. The distributed acoustic sensing (DAS) array is indicated by the nearly vertical black dotted lines along the two boreholes, and the geophone array by dark green diamonds

2.2 Distributed acoustic sensing system design and installation

The DAS system was implemented as a scalable solution for continuous, high-resolution monitoring. The installation uses Silixa's Carina sensing system using engineered Constellation fibres to gain two orders of magnitude lower noise floor (100x or 20 dB improvement) over that achieved with standard fibres. This step change in performance helps to improve detection sensitivity in the mining environment.

The fibre network is deployed in two nearly vertical boreholes reaching depths of 1,144 m and 1,101 m. Cables are connected in a daisy-chain configuration to a surface cabinet, eliminating the need for underground electronics at sensing points and allowing the interrogator to be housed remotely in a secure location.

Survivability during cave propagation was a key design requirement. Because the system relies on passive fibre-optic cables without underground power or communication infrastructure, fibres could be installed directly in zones where yield was expected. These areas are typically avoided by conventional sensors. Instrumenting these high-risk regions enables earlier and higher-resolution observation of damage evolution associated with cave growth.

As the cave advances and cable breakage occurs due to dislocation on faults mobilised by the cave, downstream channels become unavailable due to loss of optical continuity. To mitigate total signal loss, optical turnarounds were installed at 33, 66 and 100% of borehole depth, as illustrated in the cable layout in Figure 2.

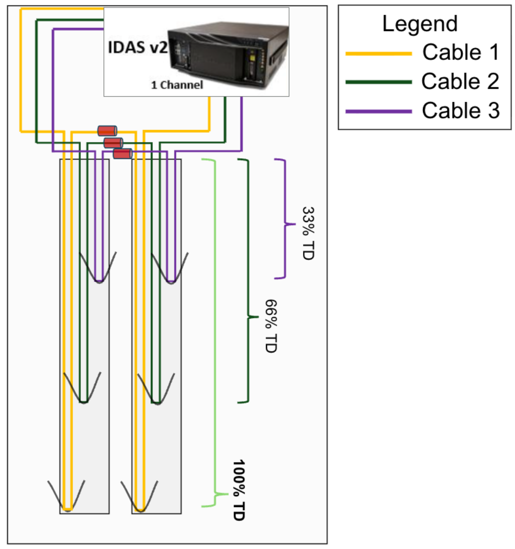

Figure 2 Installation set-up showing the cable layout, optical turnarounds and distributed acoustic sensing (DAS) interrogator

This redundancy preserves data acquisition in the upper sections even after lower segments are cut, ensuring continued monitoring throughout cave development. Although the system also supports DSS through the iDSS interrogator, analysis of continuous strain data is beyond the scope of the present study.

3 Monitoring systems and data

This study focuses on seismic processing using DAS and compares its performance with a conventional geophone-based monitoring system. For geophone-based measurements, the triggered waveforms from the system provided by Institute of Mine Seismology (IMS) are used.

3.1 Distributed acoustic sensing and geophone configurations

Figure 1 provides a visual overview of the DAS and geophone sensor arrays. A total of 398 DAS channels were employed, and sampled at 1,000 Hz with a spatial sampling interval of 5 m. This configuration was selected as a necessary compromise between signal-to-noise ratio (SNR), spatial resolution and data rate. The boreholes contained 210 and 188 channels each. The geophone system consists of 154 installed sensors (for more details see, for example, Mercier et al. [2018] and Bayar et al. [2024]), which is significantly fewer than the 398 channels in the DAS array. However, because the DAS cables are installed in an almost planar layout, the 3D monitoring volume of the DAS array (defined by the convex hull) is 3,249 times smaller than that of the geophone array. In addition, all DAS channels lie within the volume of the geophone array, occupying only 0.031% of its space. The difference between these arrays will significantly impact microseismic detection and processing of seismic events that we will show in more detail in Section 4.

3.2 Data volume and processing

Continuous high-resolution data acquisition commenced on 9 November 2023, and seismic autoprocessing on 12 June 2024. The seismic processing utilises the Bayesian Estimation of Mining-Induced Seismicity (BEMIS) processing engine (Törnman & Martinsson 2020) which supports horizontal scaling, enabling computational resources to be added on demand if data increases. DAS data volumes are significantly higher than those generated by traditional geophone systems because the triggered SEGY files (Hagelund & Levin 2017) contain information from all channels simultaneously for the triggered time window. To reduce processing costs and manage storage requirements, a prefilter was applied to the data. This filter discards traces with a SNR below a specific threshold and DAS specific noises. The strain rates were scaled with a transformation constant to approximate the observed geophone amplitudes (ground particle velocity), and two additional constants were applied to align energy and moment estimates independently, to obtain comparable magnitudes. This enables relative magnitude assessment, but this simplified method does not account for, for example, gauge-length effects necessary for the full transfer function between strain rate and ground motion (Hartog 2017). Without the transformation function, reference geophone data is required, as used here. The exported geophone data from the IMS system are limited to pre-associated waveforms, representing only a small fraction of all triggered waveforms (Törnman & Martinsson 2020). Unassociated triggered waveforms are often discarded after a retention period to reduce storage demands.

4 Seismic processing results

This section evaluates differences in microseismic results arising from sensor type and processing methodology as well as the challenges in DAS processing due to the sensor array geometry. Figures were generated in mXrap (Harris & Wesseloo 2015) using the BEMIS mXrap Extension software (Törnman 2023).

4.1 Differences in microseismic event processing

The evaluation here focuses on the impact of the sensor array geometry while keeping the seismic processing algorithms the same. Here we switch the data source between triggered seismograms from the DAS sensor array, and the triggered (and pre-associated) seismograms from the geophone sensor array, from the same time period. It is important to keep in mind the significant differences between the two sensor arrays in terms of spatial coverage, number of sensing elements, sensor characteristics, triggering logic, applied prefiltering and data limitations by pre-association mentioned in Section 3.

4.1.1 The dataset, detectability and sensitivity

Figure 3a presents the activity chart for the comparison period from 1 September 2024 to 1 October 2024. Several data gaps and system changes occurred during this interval. The dataset includes a test batch from January 2024 followed by continuous data acquisition beginning on 12 June, when automatic processing commenced.

During the January 2024 test period the cable was fully intact, and BEMIS DAS detected and located more events than the geophone-based system. However, after the first cable break at the end of May 2024, the performance of the DAS system declined. When automatic processing started on 12 June, fewer than 50% of the events detected by the geophones were identified by the DAS system (see Figure 3a). Two additional cable breaks occurred at the end of November and the end of December, further degrading the DAS array. These later periods are excluded from the comparison presented here because BEMIS processing of the geophone data was not yet available.

Although many DAS channels remained operational after each break, one reason for the reduced event count is the spatial distribution of seismicity. Most of the numerous small-magnitude events occur near the cave. When the cable breaks, the effective distance to these events increases, leading to reduced detection sensitivity and reduced location accuracy. The decrease in magnitude sensitivity is evident in the magnitude-time plot shown in Figure 3b.

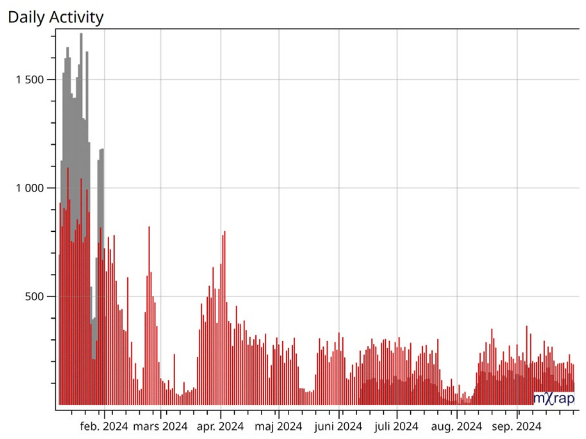

(a)

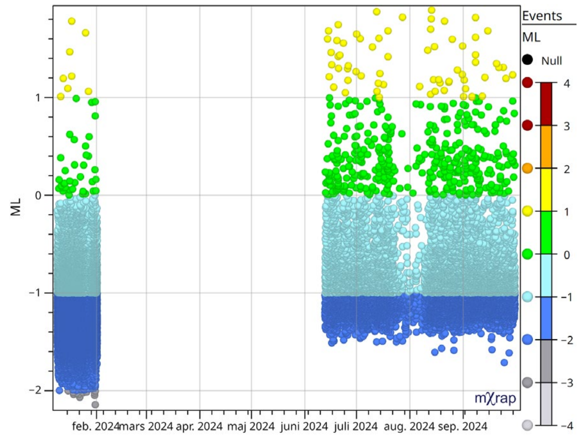

(b)

Figure 3 (a) Daily activity chart of Bayesian Estimation of Mining-Induced Seismicity events recorded by the geophone system (red) and the distributed acoustic sensing (DAS) system (grey); (b) Magnitude-time chart for DAS events, coloured by estimated magnitude. The DAS dataset includes batch data from January and continuous recordings starting on 12 June, while the geophone dataset spans from January 2014 through to 1 October 2024

4.1.2 Event location differences

Figure 4 shows BEMIS event locations for P0 over the comparison period. The first and second columns correspond to DAS array data and geophone array data, respectively. The events are coloured by the distance to a matched event between the systems, where matching is based on connecting two events with the smallest origin times difference within 10 ms. Note, however, that this matching is not perfect and outliers may be present in the figures.

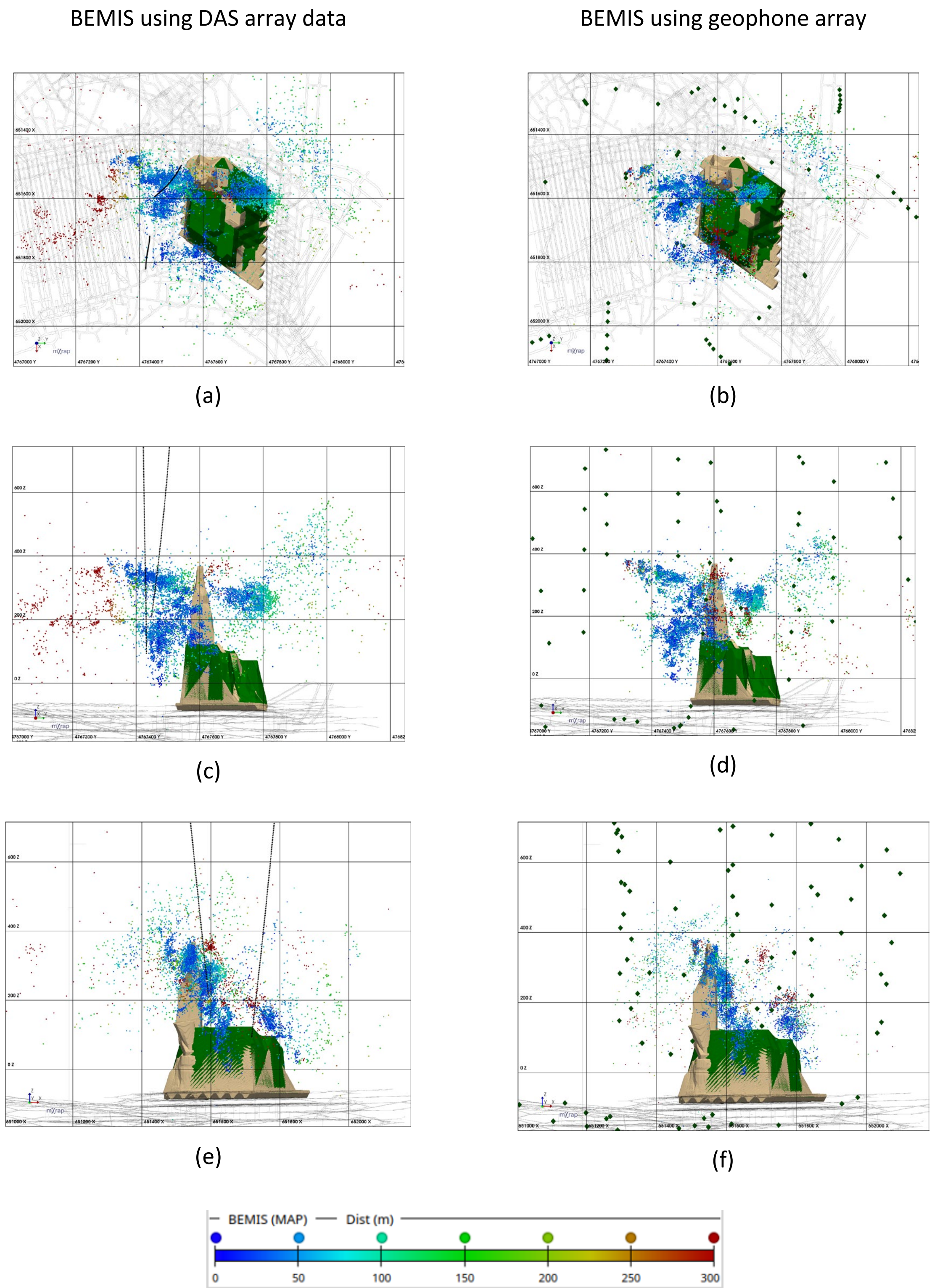

Figure 4 **(a, c, e) Comparison of hypocentre locations for events independently estimated using the distributed acoustic sensing array (i.e. left panels); (b, d, f) the geophone array (i.e. right panels) with the Bayesian Estimation of Mining-Induced Seismicity processing algorithm. The top row (a, b) shows the horizontal XY view, and the middle (c, d) and bottom (e, f) rows show the vertical YZ and XZ views, respectively. Events are coloured by distance to their corresponding matched event from the other system, where dark red dots are above a 300 m distance**

More than half of the matched events are less than 50 m apart and more than 80% of the events are less than 100 m apart (see Figure A1a in the Appendix for more statistics of event location differences). Despite the significant differences in sensor array coverage, where the DAS only covers 0.031% of the monitoring volume, a surprisingly good agreement between event locations is apparent. A few interesting discrepancies in Figure 4, coloured in dark red (i.e. more than a 300 m difference), are worth mentioning; these are the result of mirroring effects caused by the near-planar DAS array.

In Figure 5 a selection box is applied to these DAS events, and a similar mirror pattern is observed on the opposite side of the fibre for the selected matched geophone events.

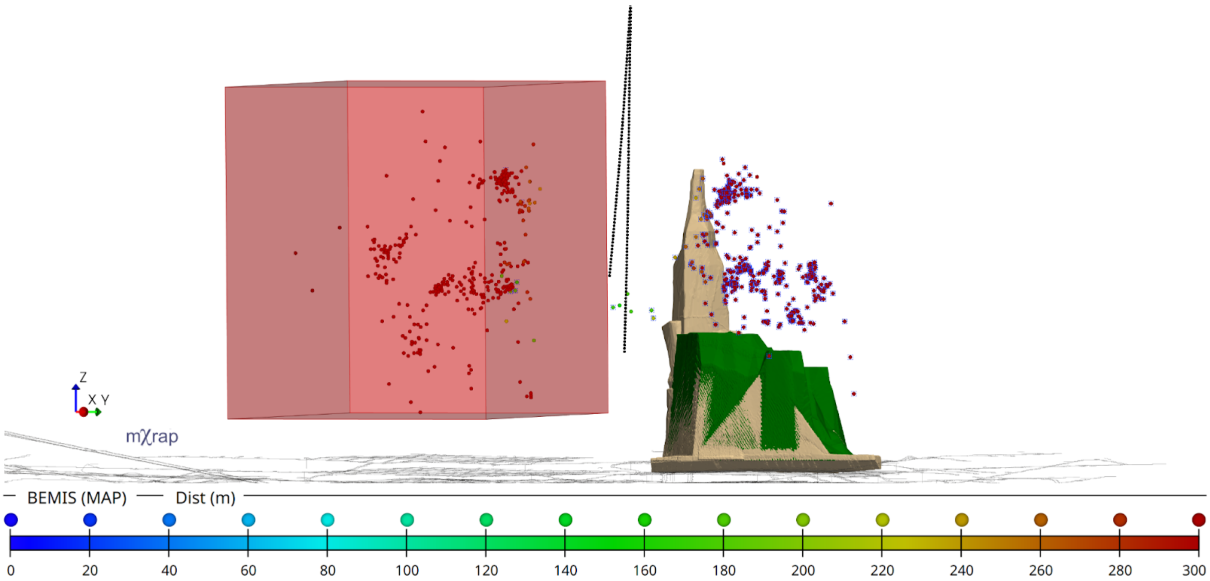

Figure 5 Corresponding matched geophone event locations for selected distributed acoustic sensing events (highlighted in the red selection box) are shown on the opposite side of the fibres (black dots), exhibiting a clear mirror-image pattern between the two datasets

Another interesting 'shadowing' effect appears to the right of the chimney in Figures 4(a–d), at Y > 4,767,600, where clusters on the cave's back side (if seen from the DAS array) are more diffuse than in the geophone data. There are two main reasons for this: the sensitivity is considerably lower on this side as the array is lacking 3D coverage, and self-calibration far outside the monitoring volume is less effective where it cannot utilise full sensor coverage.

4.1.3 Magnitude and source parameter comparison

Although the data were not properly transformed from strain to velocity, as mentioned in Section 3.2, a strong correlation between the estimated magnitudes is observed in Figure 6d. For the matched events there is good agreement in energy and moment estimates between the two systems; however, a systematic difference is apparent for the estimated corner frequencies, with DAS generally providing higher values. This discrepancy occurs despite both recording systems adopting a fixed S-wave Q value of 100, which is within the expected range for these mining depths (see, for example, Törnman et al. [2021] and references therein). Additionally, Figure A1b in the Appendix shows that more than 80% of the matched events show a magnitude difference of less than 0.4 when comparing moment magnitudes calculated using the same scale ($0.666 \times \log_{10}[\text{Moment}] - 6.066$) in both systems.

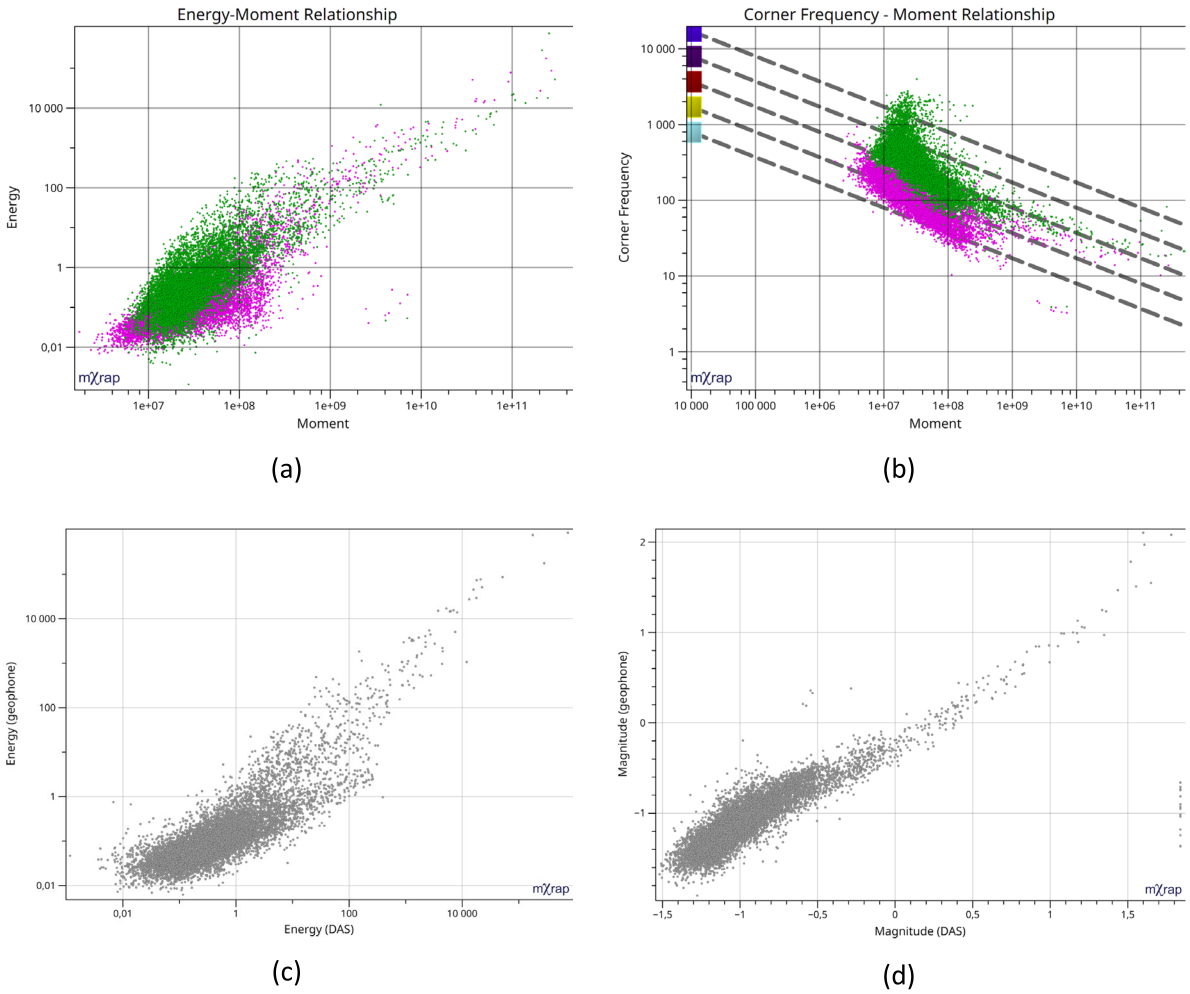

Figure 6 Comparison of source parameters for matched events recorded by the geophone (magenta points) and distributed acoustic sensing (DAS) (green points) systems: (a) The relationships between energy and seismic moment; (b) relationship between corner frequency and seismic moment; (c) comparisons of radiated energy; (d) magnitudes between the two arrays

4.2 Event processing results

This section presents the results of DAS-based event processing, focusing on event localisation under suboptimal array geometry, associated mirroring effects and channel loss due to cable damage caused by structure dislocations associated with cave propagation. The section concludes with a review of pre-DAS seismic activity to provide context and validation.

4.2.1 Impact of suboptimal geometry and mirroring effects

An optimal DAS array design for locating microseismic events is difficult to define in a universal way as it depends on site-specific constraints such as mine layout, drilling possibilities and available infrastructure. That said, to reduce spatial symmetries and avoid location ambiguities, array configurations that are close to linear or planar should be avoided. In addition, the convex hull of the array should ideally cover the full 3D monitoring volume of interest and provide sufficient sensor density to enable reliable detection and location of seismic events.

The network geometry in this study, consisting of two nearly parallel boreholes, presents a significant challenge for event localisation. This configuration essentially forms a planar array, which lacks the azimuthal coverage required to uniquely constrain event locations in 3D. This suboptimal geometry introduces an ambiguity known as the mirroring effect, where a seismic source on one side of the array plane produces travel times almost identical to a source at the mirrored position on the opposite side. Note that this effect is also present in geophone-based arrays (see, for example, Martinsson [2013]; Törnman et al. [2024]). Consequently, some event locations may converge to local minima in the mirrored region, particularly for smaller events where the SNR is lower. In these situations, the Bayesian framework offers a distinct advantage. By estimating the full probability distribution rather than a single deterministic point, the method allows for the visualisation of all plausible hypocentres (Martinsson 2013), thereby explicitly quantifying the spatial uncertainty introduced by the planar array geometry.

Three distinct cases illustrating the impact of array geometry on event localisation are presented below.

Case I: Figures 7c and d illustrate typical event locations on either side of the monitoring plane. For these events, most of the DAS channels were triggered across both boreholes. The slight deviation in borehole trajectories breaks the perfect planar symmetry, thereby solving the spatial ambiguity and providing the hypocentre distribution of the event to one side of the array. Recordings and posterior predictive arrival time distributions for one of these strong events (c) are shown in Figure 8b.

Case II: In Figure 7b a smaller event triggered only a subset of the channels that are more aligned to a plane. This increases the ambiguity and creates a mirroring type event uncertainty with two credible regions on opposite sides of the plane. Recordings and posterior predictive arrival time distributions for the event are shown in Figure 8a.

Case III: Figure 7a illustrates a more extreme scenario frequently encountered with weaker events occurring in close proximity to a single borehole. In this instance only a small subset of channels along the nearest fibre is triggered, reducing the array to a linear configuration. This introduces a rotational ambiguity where the radial distance to the fibre is constrained but the azimuth is not, resulting in a torus-shaped uncertainty region. Notably, one section of the torus exhibits higher credibility; this asymmetry is directed by the data-driven self-calibration, which provides a more informative velocity description on the side of the plane previously illuminated by seismic events (as described in Törnman & Martinsson [2020]; Törnman et al. [2024]).

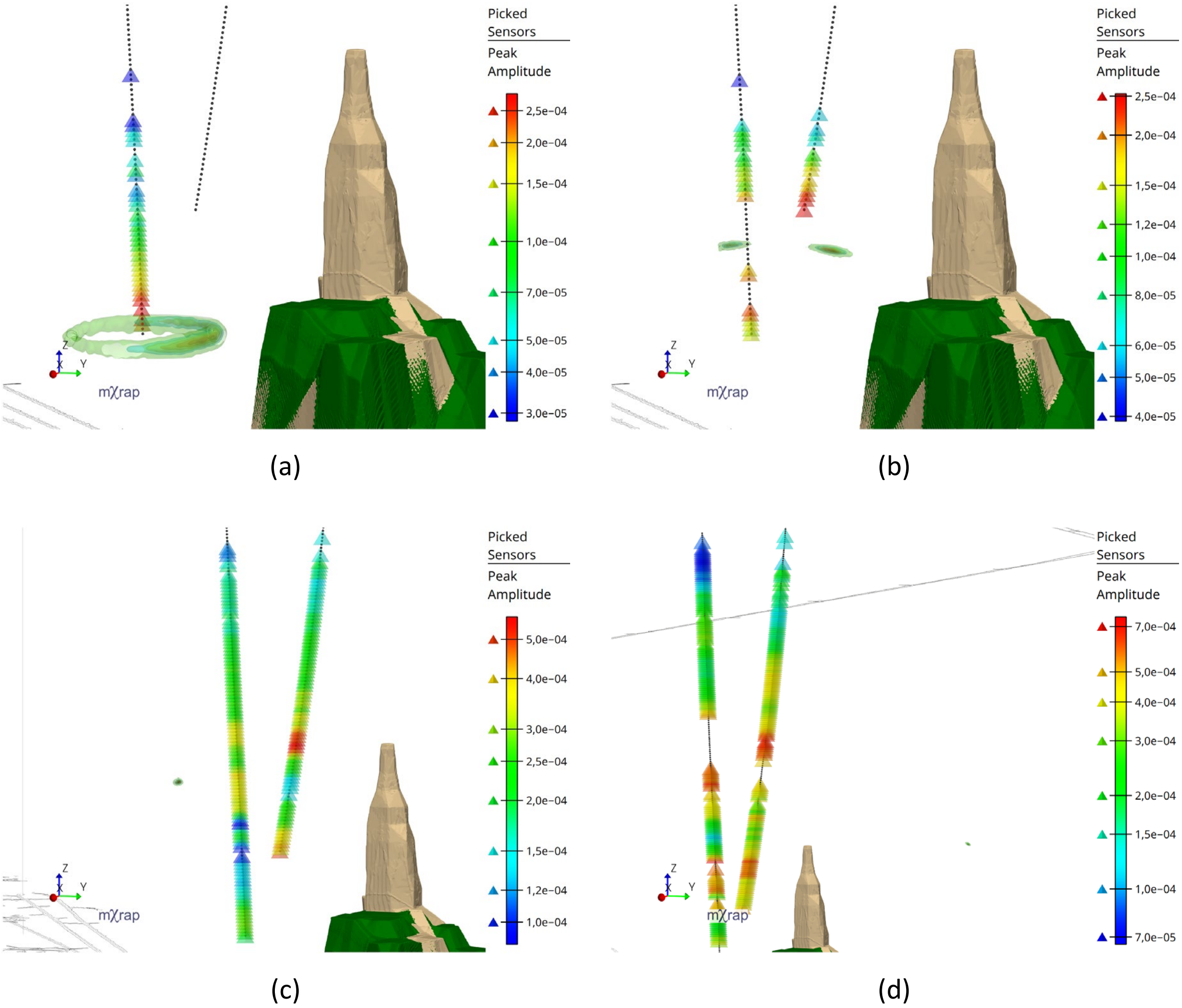

Figure 7 Credible regions of the hypocentre distributions (green contours) for four events, with sensors coloured according to the peak amplitude of the waveform. The first row shows two smaller events: (a) ML[LR2.1] = −1.65; (b) ML = −1.51. The second row shows two slightly larger events: (c) ML = −0.67; (d) ML = −0.26

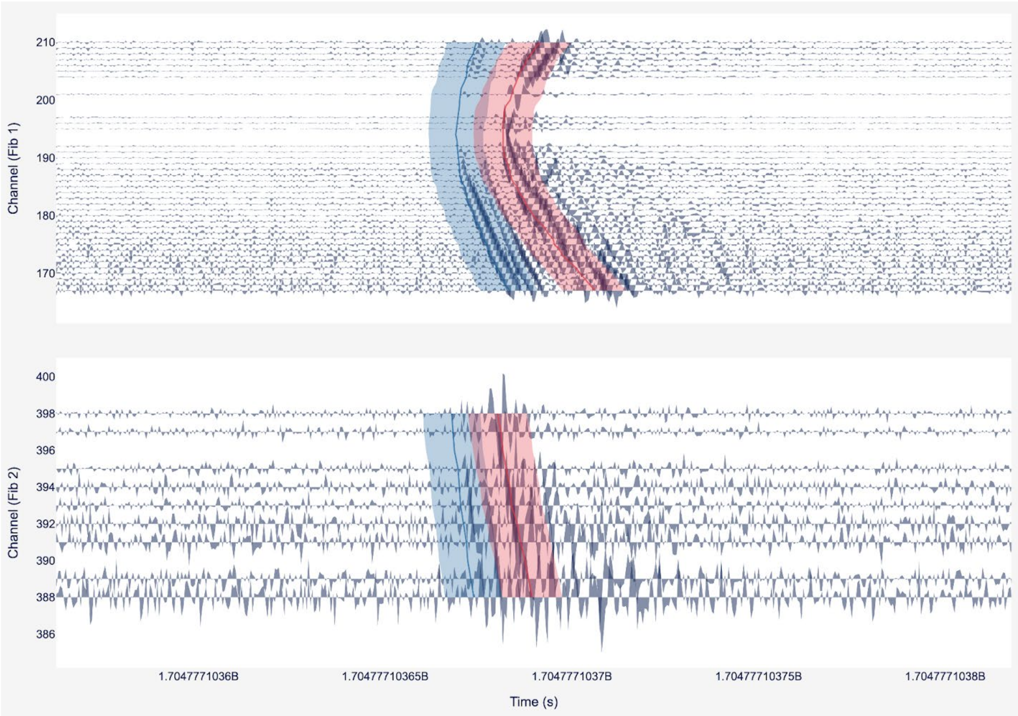

(a)

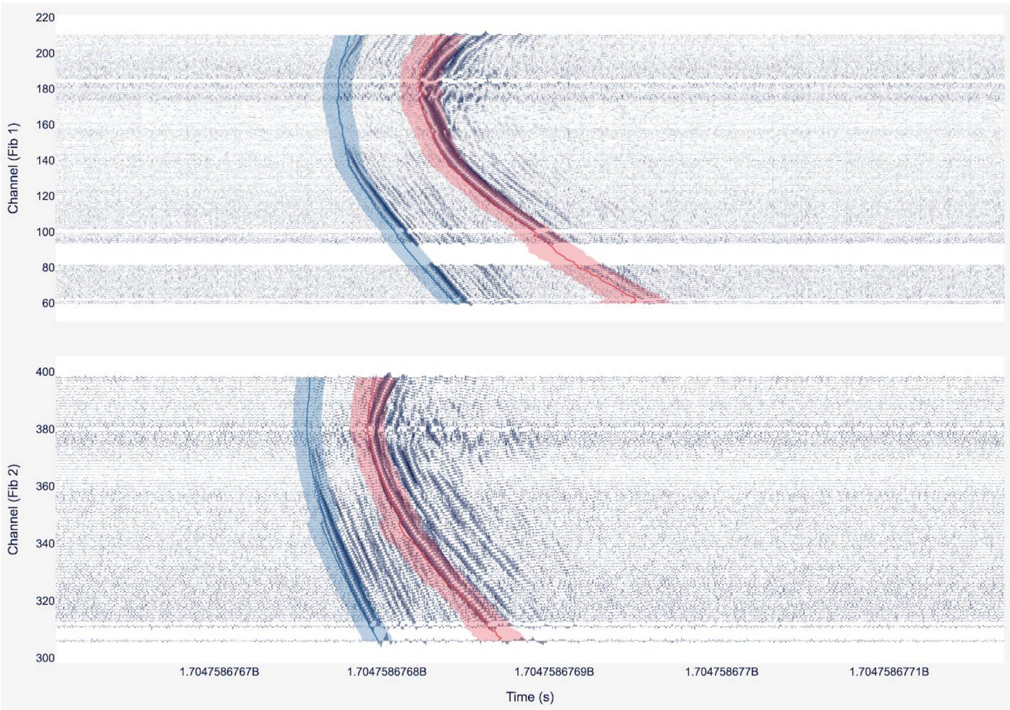

(b)

Figure 8 Triggered waveforms recorded on each fibre: (a) Corresponds to the mirroring event shown in Figure 7b; (b) Corresponds to the event shown in Figure 7c. The blue and red hyperbolas, together with their corresponding shaded bands, represent the median arrival times and the 95% uncertainty bounds derived from the hypocentre distribution represented in green and shown in Figure 7. Figures are created with the distributed acoustic sensing add-on in the Bayesian Estimation of Mining-Induced Seismicity Quake Monitor (Huber 2023)

4.2.2 Seismic activity prior to distributed acoustic sensing installation

Figure 9 shows the seismic activity around P0 before the DAS array was commissioned. Results from two independent geophone-based processing solutions are included to reinforce the interpretation: BEMIS (9a) and the conventional processing workflow (9b). Both solutions exhibit consistent spatial patterns, with correlated event locations and well-defined seismic clusters in proximity to the fibre, which experienced its first breakage a few months later (May 2024). The comparison also allows assessment of whether the limited pre-associated data affected BEMIS processing.

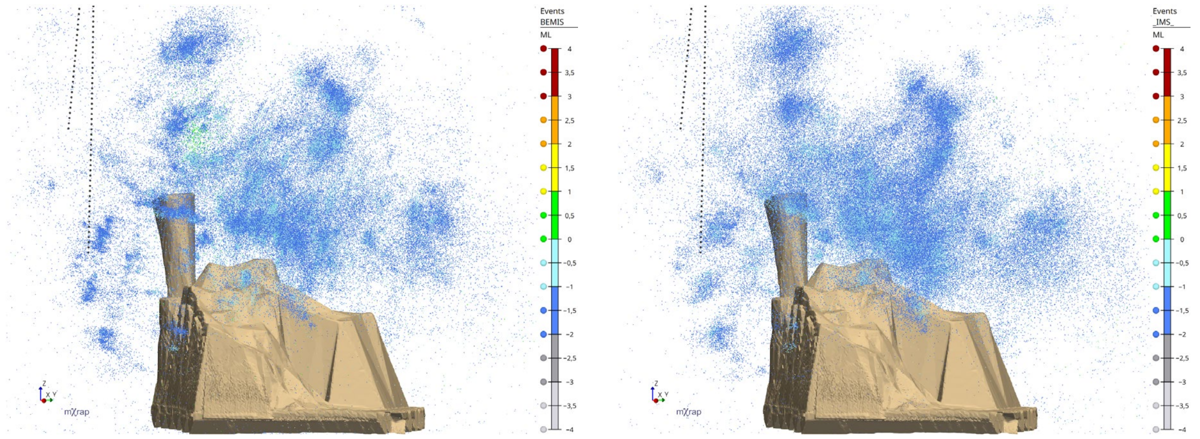

(a) (b)

Figure 9 Perspective views of seismic events recorded around Panel 0 prior to distributed acoustic sensing (DAS) commissioning Hypocentre locations for a similar number of accepted events Bayesian Estimation of Mining-Induced Seismicity (a) and conventional processing (b), for the period 1 January 2023 to 1 November 2023. Black dots on the left of the cave show the DAS channels

5 Conclusion

The large-scale deployment of distributed acoustic sensing (DAS) at the Oyu Tolgoi Panel 0 block cave confirms that DAS is a feasible and scalable tool for continuous, high-resolution seismic monitoring in active mining environments. By utilising a passive, inexpensive fibre-optic architecture equipped with optical turnarounds for redundancy, the system successfully captured the microseismic response of the rock mass and remained operational even as cave propagation caused structural dislocations that damaged sections of the cables. Fibre-optic sensing demonstrates strong potential as a complementary tool to conventional geophone networks, offering significant operational benefits by eliminating the need for complex underground power, communication infrastructure, and time synchronisation near the sensing points. The application of automated Bayesian processing on the dense DAS array shows that event localisation is comparable and source parameters correlated well with the estimates from the geophone data, even when constrained by a suboptimal DAS sensor geometry. However, it is important to note that the DAS array design is critical to maximising the DAS location accuracy and sensitivity. The near-planar layout of the boreholes lacked 3D azimuthal coverage, which introduced some spatial ambiguities and 'mirroring effects' in event localisation. Overall, this study confirms that DAS can deliver reliable, high-resolution seismic monitoring in active block caves, provided that array geometry, calibration strategy and processing workflows are carefully designed. When integrated thoughtfully with conventional systems, fibre-optic sensing represents a powerful next-generation tool for monitoring rock mass response during large-scale mining operations.

Acknowledgement

The authors gratefully acknowledge the support of Oyu Tolgoi (OT) and Rio Tinto in providing access to mine data, operational insights and technical discussions that have been valuable to this study. The contributions of the OT and Rio Tinto teams in enabling site information, geotechnical context and constructive feedback are sincerely appreciated.

Use of artificial intelligence disclosure statement

In the preparation of this work, the authors used ChatGPT (OpenAI, GPT-5) to assist with language editing and to condense text where it was overly long. The authors have reviewed the content and edited it where required and take full responsibility for said content.

Appendix

The appendix contains additional figures that provide further detail and supplementary evidence supporting the results presented in Section 4.

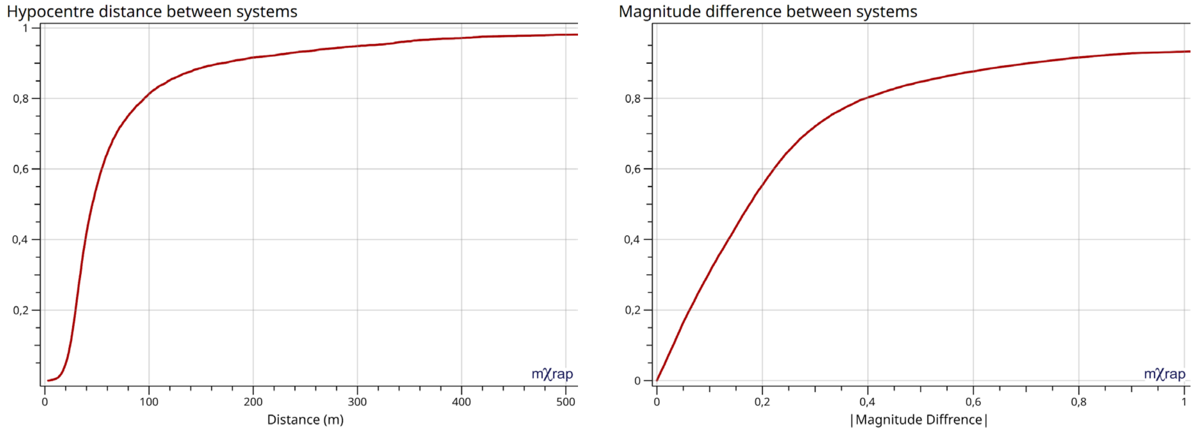

(a) (b)

Figure A1 Cumulative plots of the location differences (a) and magnitude differences (b) between matched event estimates derived from the distributed acoustic sensing and geophone systems, processed using Bayesian Estimation of Mining-Induced Seismicity

References

Bayar, E, Simanjuntak, K, Birch, D, Mardiansyah, F & Purwanto, H 2024, 'Seismological data and analysis for the early stages of block caving', in D Johansson & H Schunnesson (eds), *MassMin 2024: Proceedings of the International Conference & Exhibition on Mass Mining*, Luleå University of Technology, Luleå, pp. 893–908, https://doi.org/10.36487/ACG_repo/2435_G-02

Hagelund, R & Levin, SA (eds) 2017, *SEG-Y revision 2.0: Data Exchange Format*, Society of Exploration Geophysicists, https://seg.org/wp-content/uploads/2025/11/seg_y_rev2_0_mar2017.pdf

Harris, PC & Wesseloo, J 2015, mXrap, version 5, computer software, Australian Centre for Geomechanics, Perth, https://mxrap.com

Hartog, AH 2017, *An Introduction to Distributed Optical Fibre Sensors*, CRC Press, Boca Raton.

Huber, E 2023, *BEMIS Quake Monitor*, version 1, computer software, RockSigma, Luleå, https://www.rocksigma.com

Lindsey, NJ, Martin, ER, Dreger, DS, Freifeld, B, Cole, S, James, SR, … Ajo-Franklin, JB 2017, 'Fiber-optic network observations of earthquake wavefields', *Geophysical Research Letters*, vol. 44, pp. 11,792–11,799, https://doi.org/10.1002/2017GL075722

Martinsson, J 2013, 'Robust Bayesian hypocentre and uncertainty region estimation: the effect of heavy-tailed distributions and prior information in cases with poor, inconsistent and insufficient arrival times', *Geophysical Journal International*, vol. 192, no. 1, pp. 1156–1178.

Mercier, J-P, van As, A, Carlson, C & Tumur-Ochir, B 2018, 'Microseismic monitoring of the Oyu Tolgoi Hugo North Lift 1', in Y Potvin & J Jakubec (eds), *Caving 2018: Proceedings of the Fourth International Symposium on Block and Sublevel Caving*, Australian Centre for Geomechanics, Perth, pp. 823–834, https://doi.org/10.36487/ACG_rep/1815_65_Mercier

Törnman, W 2023, *BEMIS mXrap Extension*, version 1, computer software, RockSigma, Luleå, https://www.rocksigma.com

Törnman, W & Martinsson, J 2020, 'Reliable automatic processing of seismic events: solving the Swiss cheese problem', in J Wesseloo (ed.), *UMT 2020: Proceedings of the Second International Conference on Underground Mining Technology*, Australian Centre for Geomechanics, Perth, pp. 155–172.

Törnman, W, Martinsson, J & Dineva, S 2021, 'Robust Bayesian estimator for S-wave spectra, using a combined empirical Green's function', *Geophysical Journal International*, vol. 227, no. 1, pp. 403–438.

Törnman, W, Martinsson, J & Svanberg, E 2024, 'Enriching seismic data with noise and blasts and the importance of credibility', in P Andrieux & D Cumming-Potvin (eds), *Deep Mining 2024: Proceedings of the 10th International Conference on Deep and High Stress Mining*, Australian Centre for Geomechanics, Perth, pp. 207–216, https://doi.org/10.36487/ACG_repo/2465_08